# Phase error correction method based on the Gaussian filtering algorithm and intensity variance*

**GU Qian-qian** (谷倩倩), **LÜ Shan-shan** (吕珊珊)**, **JIANG Ming-shun** (姜明顺), **ZHANG Lei** (张雷), **ZHANG Fa-ye** (张法业), **SUI Qing-mei** (隋青美), **and JIA Lei** (贾磊)
*School of Control Science and Engineering, Shandong University, Jinan 250061, China*

(Received 15 January 2020; Revised 1 August 2020)


To overcome the invalid phase and phase jump phenomenon generated during the phase unwrapping, a phase error correction method based on the Gaussian filtering algorithm and intensity variance is proposed in this paper. First, a threshold of fringe intensity variance is set to identify and clear the phase in the invalid region. Then, the Gaussian filtering algorithm is employed to correct the phase order at the fringe junction, and then the absolute phase is corrected. Finally, the phase correction experiments of different geometric objects are carried out to verify the feasibility and accuracy of the proposed method. The method proposed in this paper can be extended to the correction of absolute phase error obtained by any coding method.

**Document code:** A **Article ID:** 1673-1905(2021)04-0221-5
**DOI** https://doi.org/10.1007/s11801-021-0009-6

Structured light-based three-dimensional (3D) measurement, which features none contact, high speed and high accuracy, has been widely applied to 3D model reconstruction, 3D surface contour measurement, automated testing and other fields[1,2]. It realizes 3D measurement by extracting the phase information from the deformed grating stripe. However, the Fourier transform profilometry (FTP) or the phase-shifting profilometry (PSP) can only get the relative phase wrapped in the range of [−π, π], which is not unique. Thus, phase unwrapping is necessary to obtain a continuous absolute phase[3,4].

Phase unwrapping is important for the 3D measurement based on structured light. Scholars have developed many phase unwrapping algorithms, which can be classified into spatial and temporal categories[5]. The spatial category restores the absolute phase based on the phase of the previous pixel. The accumulation of errors may be generated because of the phase jump caused by the noise, shadow and other invalid pixels in the real measurement, which hence reduces the reliability. The temporal category can effectively avoid error transmission, has strong robustness, and is suitable for objects whose surface is discontinuous or with abrupt height changes. It mainly includes dual-frequency heterodyne, Gray-code and phase-coding methods. Dual-frequency heterodyne method requires fewer projected images, while its heterodyne operation will magnify the error in the relative phase, resulting in an unsmooth phase curve[6-9]. The gray-code method has 2π jumps, which caused by the gray-code and relative phase cannot change synchronously[10-13]. Similar to the Gray-code method, the phase-coding method still contain unwrapping error at the boundary between adjacent codewords though the designed codewords embedded in phase[14,15]. Such error must be removed to obtain accurate absolute phase. Zhang et al[16] eliminated the error by monotonicity detection. Zhang et al[17] proposed a complementary Gray-code method, using the different and complementary boundary locations of the traditional and additional codes. Zheng et al[18] adopted an adaptive median filter to effectively remove unwrapping errors. It should be noted that the erroneous pixel detection process is a little time-consuming.

Aiming at the above problems, this paper combines four-step phase-shifting with gray-code to realize the phase unwrapping. It further develops a method to correct phase error based on the Gaussian filtering algorithm and intensity variance, which effectively avoids unwrapping errors and maintains the high accuracy of phase unwrapping.

The phase-shifting method projects multiple standard sinusoidal grating images with the same phase increment on the surface of the measured object. When being modulated by the height of the measured object, the grating images tend to be distorted. The analysis and processing of the distorted images will help identify the

* This work has been supported by the National Natural Science Foundation of China (Nos.61873333 and 61903225), the Fundamental Research Funds of Shandong University in China (No.2018JCG06), the Shandong Provincial Natural Science Foundation in China (Nos.ZR2017PEE023 and ZR2017BF007), the National Key Research and Development Project (No.2018YFE02013), the Key Research and Development Plan of Shandong Province (No.2019TSLH0301), and the Young Scholars Program of Shandong University (No.2016WLJH30).
** E-mail: sdulvshanshan@163.com

distribution of the relative phase. The measurement principle of the standard four-step phase-shifting method is illustrated. The light intensity of the distorted grating images modulated by the measured object can be expressed as

$$I_i(x,y) = a + b\cos[\varphi(x,y) + \delta_i], \quad (1)$$

where $a$ is the light intensity of the background, $b$ is the modulated light intensity, $\varphi(x, y)$ is the relative phase, and $\delta_i$ is the initial phase of the $i$th image.

Ideally, the light intensity of the projected grating image is consistent with the standard sinusoidal distribution. When the four-step phase-shifting method is used to calculate the relative phase of the grating image, the phase shift of each step is π/2. That is, four grating images with an initial phase of 0, π/2, π and 3π/2 respectively should be projected. The light intensity is expressed as

$$I_1(x, y)=a+b\cos[\varphi(x, y)], \quad (2)$$

$$I_2(x, y)=a+b\cos[\varphi(x, y)+\pi/2], \quad (3)$$

$$I_3(x, y)=a+b\cos[\varphi(x, y)+\pi], \quad (4)$$

$$I_4(x, y)=a+b\cos[\varphi(x, y)+3\pi/2]. \quad (5)$$

The corresponding relative phase can be obtained from the above four equations:

$$\varphi(x,y) = \arctan\left(\frac{I_4 - I_2}{I_1 - I_3}\right), \quad (-\pi \le \varphi \le \pi). \quad (6)$$

According to Eq.(6) and the properties of the arctangent function, the relative phase is wrapped in the range of [−π, π]. Thus, phase unwrapping is necessary to obtain a continuous absolute phase.

Gray code is a typical non-weighted code and only one binary bit is different between two adjacent gray codes. Hence, there is only one bit jump in the gray code when the state changes, which improves the decoding accuracy and its reliability. In addition, compared with the binary-code fringe pattern with the same period, the gray-code fringe pattern has fewer boundary lines, thus mitigating the boundary effect of the fringe and reducing measurement errors.

The gray-code method projects $m$ binary coding patterns to the measured object, dividing the surface of the object into $2^m$ regions. Each pixel of the relative phase corresponds to a gray code. Since the gray code cannot be directly calculated, it is converted to the corresponding binary code and then to the decimal fringe order $n$. Combined with the relative phase $\varphi(x, y)$, the absolute phase $\Phi(x, y)$ can be obtained, which can be expressed as

$$\Phi(x, y)=\varphi(x, y)+2\pi\cdot n(x, y). \quad (7)$$

Take three projected gray-code stripe patterns as an example. If 0 corresponds to black and 1 corresponds to white, then three gray-code stripe patterns are 10, 1 001, and 10 011 001, respectively. The measured object is divided into eight regions. The corresponding gray code of each region is $G$, and its conversion relationship with binary code $B$ and fringe order $n$ is shown in Fig.1.

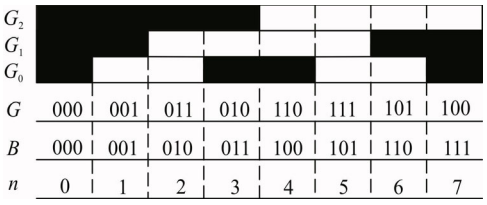


**Fig.1 The conversion relation between gray code, binary code and fringe order**

If each region is required to correspond to a unique fringe order $n$, then the minimum fringe width of the gray-code stripe pattern must be equal to the period of the phase-shifting grating image. It will ensure that the fringe order changes synchronously with the relative phase. In this way, an accurate phase unwrapping is achieved.

In the real measurement, the 3D measurement system based on structured light is extremely susceptible to factors of the external environment, resulting in some errors in the experimental results. In order to obtain ideal experimental results, these errors must be eliminated. There are two main sources of errors: background noise and 2π jumps. The former is caused by the light projected onto the background during the experiment, which is invalid information to be filtered out, as shown in Fig.2(a). The latter originates from the binarization of gray-code stripe patterns. Due to the influence of external environmental factors, pixel deviation is generated at the fringe boundary of gray-code stripe patterns during binarization. As a result, the gray-code and relative phase cannot change synchronously, causing the phase jump of the absolute phase at the position of 2π, as shown in Fig.2(b).

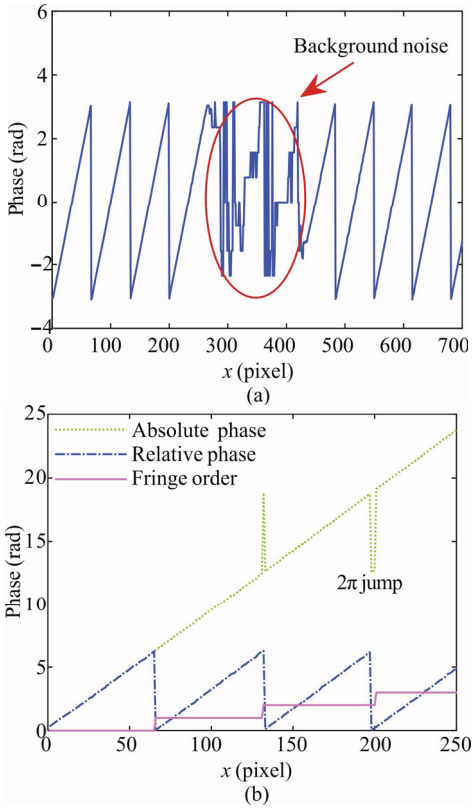


**Fig.2 (a) The background noise in relative phase; (b) The cause of 2π jumps**

During the calculation of the relative phase by the phase-shifting method, the change of the light intensity of the sinusoidal grating fringe projected on the background is much smaller than that on the measured object. According to this feature, the variance of the gray value of $k$ deformed grating images can be calculated by Eqs.(8) and (9), and an appropriate threshold is selected according to $s^2$. Background noise is eliminated by removing pixels whose $s^2$ is less than the threshold, as shown in Fig.3.

$$\bar{I}=\frac{1}{k}\sum_{i=1}^{k}I_i\,, \tag{8}$$

$$s^2=\frac{1}{k}\sum_{i=1}^{k}(I_i-\bar{I})^2\,, \tag{9}$$

where $I_i$ is the gray value of the $i$th deformed grating image, $I$ is the average gray value of $k$ deformed grating images, and $s^2$ is the variance of the gray value of $k$ deformed grating images.

The method of selecting threshold based on gray value cannot effectively identify invalid pixels with large gray value, while the proposed method can effectively solve this problem. Therefore, the method based on intensity variance is more effective.

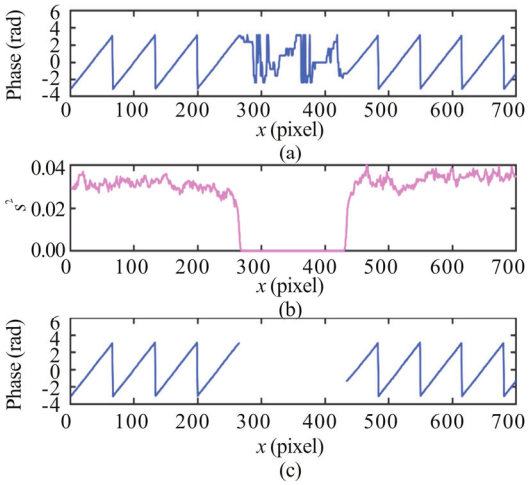


**Fig.3 The correction of background noise: (a) Relative phase before correction; (b) $s^2$; (c) Relative phase after correction**

The 2π jumps in the absolute phase can be smoothed by Gaussian filter designed as

$$h=\text{fspecial('gaussian', } p,\ \sigma), \tag{10}$$

$$\Phi'=\text{imfilter}(\Phi,\ h), \tag{11}$$

where $\Phi$ and $\Phi'$ denote the absolute phase before and after the Gaussian filtering, respectively, $h$ is the designed Gaussian filter, $p$ is the template size of the filter, and $\sigma$ is the standard deviation of the filter.

In Gaussian filtering, the value of the center pixel of the template is replaced with the weighted average gray value of the pixels in the neighborhood that is determined by the template. Errors exist in the absolute phase value after Gaussian filtering, resulting in low accuracy. Therefore, the absolute phase must be recalculated by Eqs.(12) and (13). An appropriate Gaussian template and a suitable $\sigma$ are selected to ensure that the 2π jump error is corrected to the range of (−π, π) by Gaussian filtering. For a Gaussian filter, the most important parameter is the standard deviation $\sigma$, which determines its smoothing ability. The larger the standard deviation $\sigma$, the better the smoothing ability of the filter. In general, the template size of the Gaussian filter $p$ is set to $4\sigma+1$. In this way, the jump can be eliminated perfectly. Then the accurate absolute phase can be obtained, as shown in Fig.4.

$$N=\text{round}\left(\frac{\Phi'-\varphi'}{2\pi}\right), \tag{12}$$

$$\Phi''=\varphi'+2\pi N, \tag{13}$$

where round(·) is the rounding function, $N$ is the fringe order after correction, $\varphi'$ is the relative phase after the background noise is eliminated, and $\Phi''$ is the absolute phase after the correction of 2π jumps.

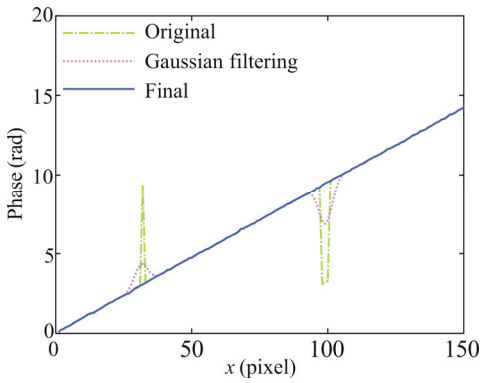


**Fig.4 The correction of 2π jumps in absolute phase**

The 3D measurement system based on structured light is composed of a projection device, an image acquisition device, a control and data processing device, and a measured object. The system is depicted in Fig.5.

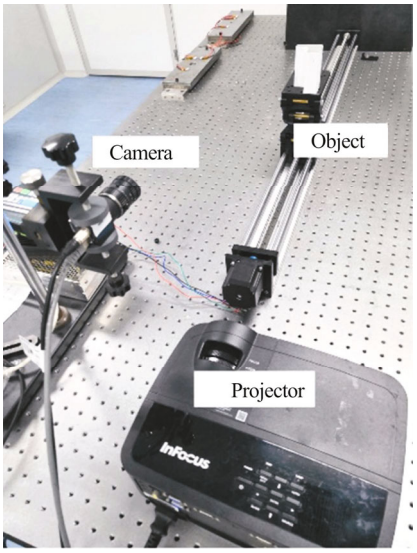


**Fig.5 The 3D measurement system**

The digital projector (IN2128HDx, 1 920×1 080) is used as the projection device, which sequentially projects the grating images and the gray-code stripe patterns on the surface of the measured object. The camera (MER-500-14GM, 2 592×1 944) is used as the image acquisition device to acquire images modulated by the measured object and transmit them to the computer. As the control and data processing device, the computer controls the camera to collect images on the one hand, and analyzes and processes the collected data on the other.

In this experiment, the fan blades are to be measured, and the phase unwrapping is achieved by the combination of four-step phase-shifting with gray-code. The six gray-code stripe patterns and four grating images used in the experiment are generated by Matlab. The generated images are projected on the surface of the fan blades by a projector in turn, and then the distorted grating images are collected by the camera and returned to the computer for processing.

The acquired distorted images are processed to obtain the relative phase, and the background noise is removed by the proposed method. Fig.6 displays the distribution of the relative phase before and after background noise correction. Fig.6(b) clearly demonstrates that the background noise in the relative phase is completely filtered out.

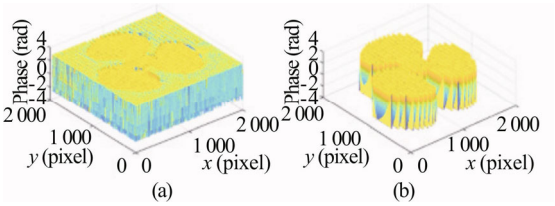


**Fig.6 Relative phase of the fan blades (a) before and (b) after background noise correction**

Afterward, the collected gray-code stripe patterns are binarized, and the fringe order $n$ of each pixel is obtained according to the conversion relationship in Fig.1. Then, the absolute phase is generated from Eq.(4) and then corrected by the 2π jump correction method based on Gaussian filtering proposed in this paper. The parameters of the Gaussian filter are set as: $p$=11, $\sigma$=2.5. The absolute phase of the fan blades in row 500 before and after 2π jumps correction is depicted in Fig.7. The number of erroneous pixels in row 500 before correction is 29, while can be reduced to 0 after correction, indicating the feasibility of the unwrapping phase error correction method based on Gaussian filtering.

In order to better illustrate the effectiveness and superiority of the proposed method, it is compared with the spatial phase unwrapping method and the dual-frequency heterodyne method. The experimental results in Fig.8 show that the spatial phase unwrapping method has phase unwrapping error at the phase jump pixels, thus not being applicable to objects with discontinuous surfaces. The absolute phase distribution curve obtained by the dual-frequency heterodyne method is not smooth. In contrast, the gray-code method after phase error correction displays no phase unwrapping error, and obtains a high-accuracy absolute phase whose distribution curve is smooth .

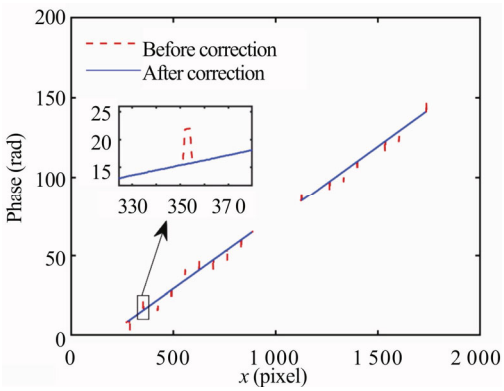


**Fig.7 Absolute phase in row 500 before and after 2π jumps correction**

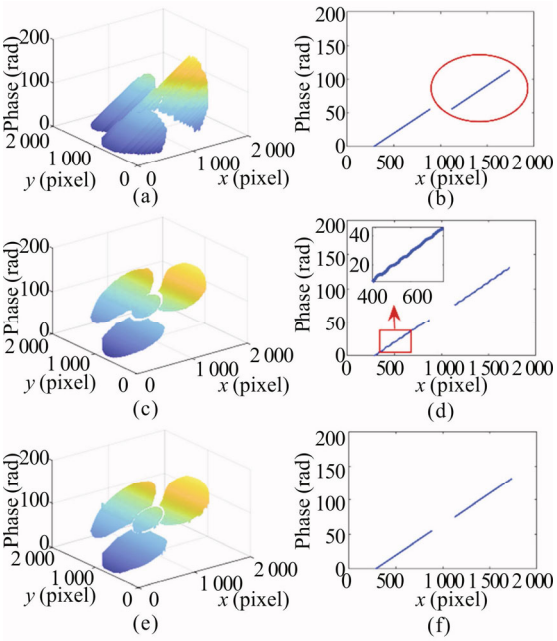


**Fig.8 Absolute phase of the fan blades: (a) The spatial phase unwrapping method; (b) Row 500 of (a); (c) The dual-frequency heterodyne method; (d) Row 500 of (c); (e) The gray-code method corrected by Gaussian filtering; (f) Row 500 of (e)**

In addition, the ladder and the sphere are respectively taken as the measured object to prove the universality of this method. The absolute phase is shown in Fig.9, which reveals that it is applicable to objects with smooth edges or surfaces with abrupt height changes.

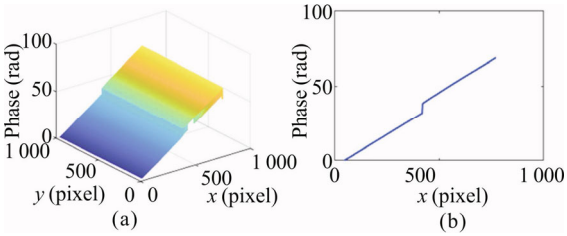

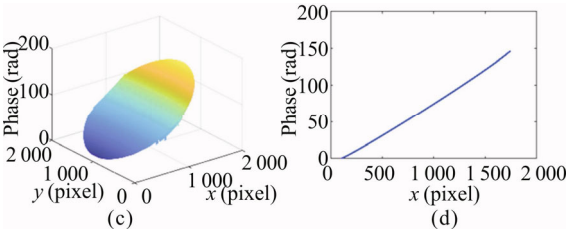


**Fig.9 Absolute phase: (a) The ladder; (b) Row 1 500 of (a); (c) The sphere; (d) Row 1 000 of (c)**

In this paper, an unwrapping phase error correction method based on the Gaussian filtering algorithm and intensity variance is proposed and elaborated. Firstly, the phase in the invalid area is cleared, followed by the correction of the fringe order at the fringe boundary. Finally, an accurate absolute phase distribution is obtained. The experimental results demonstrate that after correction, the absolute phase calculated based on the phase-shifting and gray-code patterns is more accurate than that by the traditional method. It is applicable to objets with smooth edges, discontinuous surfaces or abrupt height changes. Moreover, the phase error correction method proposed in this paper is universal for jump errors at the boundary between adjacent codewords in different phase unwrapping algorithms.

## References

[1] Zhang Song, Optics and Lasers in Engineering **106**, 119 (2018).

[2] Li Beiwen, An Yatong, Cappelleri David, Xu Jing and Zhang Song, International Journal of Intelligent Robotics and Applications **1**, 86 (2017).

[3] Emanuele Zappa and Giorgio Busca, Optics and Lasers in Engineering **50**, 1140 (2012).

[4] Zuo Chao, Feng Shijie, Huang Lei, Tao Tianyang, Yin Wei and Chen Qian, Optics and Lasers in Engineering **109**, 23 (2018).

[5] Wang Minmin, Research on Phase Extraction Algorithm for 3-D shape Measurement, Shandong University, 2018. (in Chinese)

[6] Liu Fei, Li Jiaxin, Lai Junlin and He Chunqiao, Laser & Optoelectronics Progress **56**, 011202 (2019).

[7] Wu Shuyu, Yang Yimin, Zhong Zhenyu and Lu Xingjian, Acta Optica Sinica **34**, 131 (2014). (in Chinese)

[8] Chen Songlin, Zhao Jibin and Xia Renbo, Acta Optica Sinica **36**, 155 (2016). (in Chinese)

[9] Chen Ling, Deng Wenyi and Lou Xiaoping, Optical Technique **38**, 73 (2012). (in Chinese)

[10] Yu Shuang, Zhang Jing, Yu Xiaoyang, Sun Xiaoming and Wu Haibin, Optics Communications **374**, 97 (2016).

[11] Song Qian, Chen Yue, Zhu Ronggang and Zhu Rihong, Laser & Optoelectronics Progress **51**, 115 (2014). (in Chinese)

[12] Wang Bing and Guo Ling, Computer Measurement & Control **26**, 25 (2018). (in Chinese)

[13] Zhang Qican and Wu Zhoujie, Infrared and Laser Engineering **49**, 78 (2020). (in Chinese)

[14] Fu Yanjun, Han Yonghua, Chen Yuan, Zhang Pengfei, Gui Jiannan, Zhong Kequn and Huang Caimin, Infrared and Laser Engineering **49**, 157 (2020). (in Chinese)

[15] Wang Yajun and Zhang Song, Optics Letters **37**, 2067 (2012).

[16] Zhang Song, Optics Letters **35**, 934 (2010).

[17] Zhang Qican, Su Xianyu, Xiang Liqun and Sun Xuezhen, Optics and Lasers in Engineering **50**, 574 (2012).

[18] Zheng Dongliang, Da Feipeng, Qian Kemao and Hock Soon Seah, Optics Express **25**, 4700 (2017).